ACS APPLIED MATERIALS & INTERFACES

Research Article

www.acsami.org

Role of Cobalt Content in Improving the Low-Temperature Performance of Layered Lithium-Rich Cathode Materials for Lithium-Ion Batteries

Jianwen Kou,[†,▽] Lai Chen,[†,▽] Yuefeng Su,[*,†,‡,§] Liying Bao,[*,†,‡,§] Jing Wang,[†,‡,§] Ning Li,[†] Weikang Li,[†] Meng Wang,[∥] Shi Chen,[†,‡,§] and Feng Wu[†,‡,§]

[†]School of Materials Science and Engineering, Beijing Institute of Technology, Beijing, 100081, China

[‡]Collaborative Innovation Center of Electric Vehicles in Beijing, Beijing, 100081, China

[§]National Development Center of High Technology Green Materials, Beijing, 100081, China

[∥]Advanced Manufacture Technology Center, China Academy of Machinery Science & Technology, Beijing, 100083, China

Supporting Information

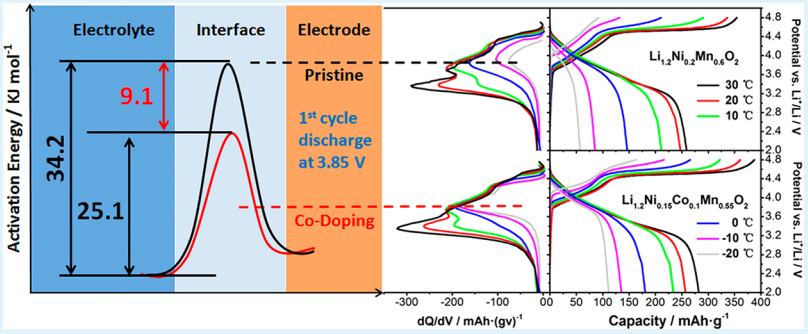

ABSTRACT: Layered lithium-rich cathode material, $Li_{1.2}Ni_{0.2-x}Co_{2x}Mn_{0.6-x}O_2$ (x = 0−0.05) was successfully synthesized using a sol−gel method, followed by heat treatment. The effects of trace amount of cobalt doping on the structure, morphology, and low-temperature (−20 °C) electrochemical properties of these materials are investigated systematically. X-ray diffraction (XRD) results confirm that the Co has been doped into the Ni/Mn sites in the transition-metal layers without destroying the pristine layered structure. The morphological observations reveal that there are no changes of morphology or particle size after Co doping. The electrochemical performance results indicate that the discharge capacities and operation voltages are drastically lowered along with the decreasing temperature, but their fading rate becomes slower when increasing the Co contents. At −20 °C, the initial discharge capacity of sample with x = 0 could retain only 22.1% (57.3/259.2 mAh g^{-1}) of that at 30 °C, while sample with x = 0.05 could maintain 39.4% (111.3/282.2 mAh g^{-1}). Activation energy analysis and electrochemical impedance spectroscopy (EIS) results reveal that such an enhancement of low-temperature discharge capacity is originated from the easier interface reduction reaction of Ni^{4+} or Co^{4+} after doping trace amounts of Co, which decreases the activation energy of the charge transfer process above 3.5 V during discharging.

KEYWORDS: *lithium-ion batteries, lithium-rich layered cathode, low-temperature performance, cobalt doping, activation energy*

1. INTRODUCTION

Rechargeable lithium-ion batteries (LIBs) are urgently needed in both portable electronic devices and large electric vehicles in our daily life, because of their higher energy density, compared to other rechargeable systems.[1−4] They are also being employed for stationary storage and utilization of intermittent renewable energies such as solar and wind.[5,6] Novel and advanced LIBs with higher energy and power density have been pursued intensively to meet these applications, and become the key to the development of advanced cathode materials.[7−9] Since the first commercialization of $LiCoO_2$ in 1980,[10] the transition-metal intercalation oxides have received major research interest as LIBs cathodes,[11] one of which is the layered lithium-rich (LLR) cathode material $xLi_2MnO_3\cdot(1-x)LiMO_2$ (where M is a transition metal).[12−15] Although these materials still suffer from intrinsic poor rate capability and modest cycle stability,[16−18] their competitive high specific capacity (ca. 250 $mAhg^{-1}$) and low cost make them more attractive than present commercialized cathode materials,[15,19] such as $LiCoO_2$, $LiFePO_4$, and $LiMn_{1/3}Ni_{1/3}Co_{1/3}O_2$.

In a general sense, the cathode materials have made great progress over the years, such that the LIBs at room temperature may have electrochemical performance adequate for use in

Received: May 24, 2015
Accepted: July 29, 2015
Published: July 29, 2015

DOI: 10.1021/acsami.5b04514
ACS Appl. Mater. Interfaces 2015, 7, 17910−17918

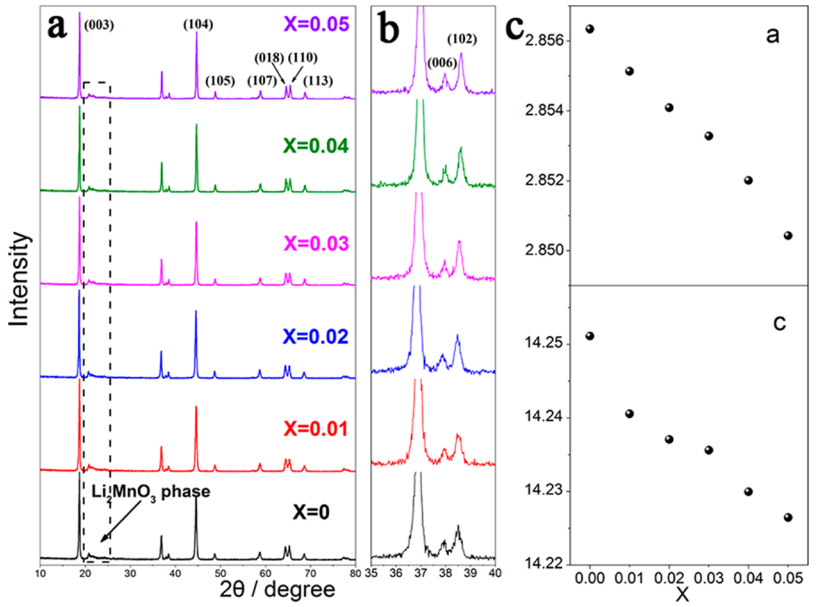

Figure 1. (a) Powder X-ray diffraction (XRD) patterns of the $Li_{1.2}Ni_{0.2-x}Co_{2x}Mn_{0.6-x}O_2$ (x = 0, 0.01, 0.02, 0.03, 0.04, 0.05) powders. (b) Enlarged view showing the separation and shape of each material's 006/102 peaks. (c) Variation in lattice parameters a and c, relative to Co content.

consumer electronics. However, their performance is poor at low temperature, limiting their applications under specific conditions.[20−23] For instance, the energy density of a commercial LIB (No. 18650) with a $LiCoO_2$ cathode at −40 °C retained only 5% of that which was retained at 20 °C.[24] Many efforts have been made to address this issue, including the development of electrolytes with higher low-temperature ionic conductivities,[25] controlling the particle size/morphology[26,27] and surface modification.[23,28−30] It is worth noting that, excluding the effects from electrolyte, the malfunction of LIBs at low temperature can be effectively mitigated, because of the decreased charge-transfer resistance of cathode/anode materials.

Recent research progresses indicate that Li^+ intercalation/deintercalation process of LLR materials is sensitive to temperature,[31,32] which is most likely associated with an increase in the interface-induced reaction impedance.[33] Nevertheless, research that focuses on improving the low-temperature electrode performances of LLR cathode materials are rarely reported. Here, we focus on investigating the role of Co^{3+} doping in influencing the low-temperature performances of LLR materials. The representative of LLR materials, $Li_{1.2}Ni_{0.2-x}Co_{2x}Mn_{0.6-x}O_2$ (x = 0, 0.01, 0.02, 0.03, 0.04, and 0.05), were employed and tested at a temperature range from 30 °C to −20 °C, to verify the possible mechanism of Co doping that affects the low-temperature properties.

2. EXPERIMENTAL SECTION

2.1. Synthesis. All the raw reagents employed here were of analytical purity grade. The lithium-rich cathode materials $Li_{1.2}Ni_{0.2-x}Co_{2x}Mn_{0.6-x}O_2$ (x = 0, 0.01, 0.02, 0.03, 0.04, and 0.05) were synthesized by a facile sol−gel method, followed by a calcination treatment. Stoichiometric amounts of $Li(CH_3COO)\cdot 2H_2O$ (5 wt % excess to offset the lithium evaporative losses), $Ni(CH_3COO)_2\cdot 4H_2O$, $Co(CH_3COO)_2\cdot 4H_2O$, and $Mn(CH_3COO)_2\cdot 4H_2O$ were dissolved in deionized water to obtain a transparent and homogeneous solution, which was then added dropwise to another solution, using citric acid as a chelating agent. The pH value of the mixed solution was adjusted to ∼7.0. The reaction solution then was heated at 80 °C with vigorous stirring to form a high viscous gel. After drying in a vacuum oven at 120 °C for 12 h, the gel was preheated at 500 °C for 5 h in air and ground after cooling. Finally, the decomposed mixture was pressed into pellets and calcined at 900 °C for 12 h to obtain well-formed powder $Li_{1.2}Ni_{0.2-x}Co_{2x}Mn_{0.6-x}O_2$. The samples obtained were named Co-0, Co-1, Co-2, Co-3, Co-4, and Co-5, corresponding to the compositions with x = 0, 0.01, 0.02, 0.03, 0.04, and 0.05, respectively.

2.2. Material Characterization. A structural analysis was carried out using X-ray diffraction (XRD) (Rigaku, Model Ultima IV-185) with a Cu Kα radiation source. The samples were scanned from 2θ = 20°−80° at a scan rate of 2° per minute. A field-emission scanning electron microscopy (FESEM) system (FEI QUANTA 250), equipped with an energy-dispersive X-ray (EDX) detector, was used to analyze the sample morphology and achieve EDX mapping. The X-ray photoelectron spectroscopy (XPS) of the sample was performed by X-ray photoelectron spectroscopy (XPS, PHI Quantera II). Before the test, the electrodes fully discharged to 3.85 V were disassembled from coin cells and rinsed with dimethyl carbonate several times in a glovebox and then dried at room temperature.

2.3. Electrochemical Tests. Electrochemical performances of the samples were examined using galvanostatic cycling with CR2025 coin-type cells. The positive electrodes were made of 80 wt % as-prepared materials powder, 10 wt % acetylene black, and 10 wt % polyvinylidene fluoride. The electrolyte was 1 M $LiPF_6$ dissolved in a (1:1 volume ratio) mixture of ethylene carbonate and ethyl methyl carbonate. The coin-type half cells were assembled in a glovebox filled with argon with lithium metal as the negative electrode and Celgard 2400 membrane as separator. The mass and diameter of our electrodes are ∼6.8−7.0 mg and 1.2 cm, respectively. Electrochemical tests (galvanostatic charge/discharge tests) were performed by a Model CT2001A Land instrument (Wuhan, China) at potential ranges of 2−4.8 V under various operating temperatures in an environmental test chamber (Giant Force). The current density of 250 mA g^{-1} was defined as 1 C rate during the test. Electrochemical impedance spectra (EIS) of the cells were also conducted using the Model CHI660 electrochemical workstation at frequencies from 10^5 Hz to 0.01 Hz with an AC perturbation signal of 5 mV. The results were analyzed using ZSimpWin software.

3. RESULTS AND DISCUSSION

3.1. Structural Characterizations. All the materials have been characterized via powder X-ray diffraction (XRD). Clearly, there are no significant differences in the crystal structures of

DOI: 10.1021/acsami.5b04514
ACS Appl. Mater. Interfaces 2015, 7, 17910−17918

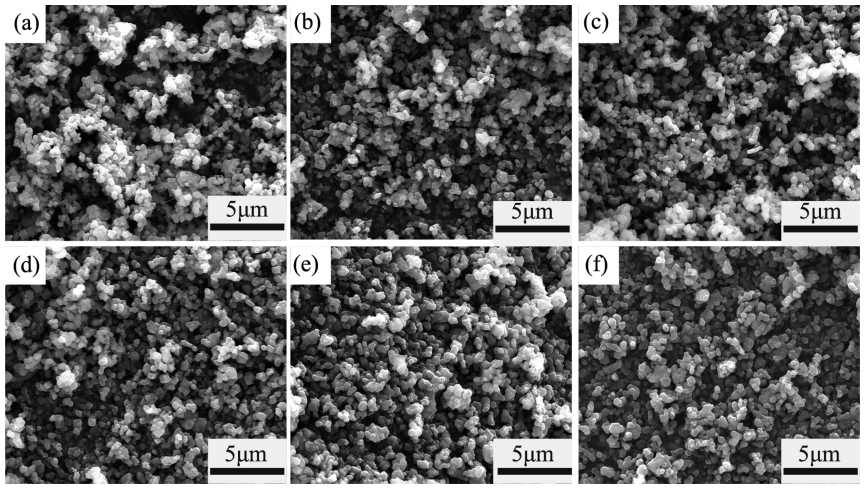

Figure 2. SEM images of the $Li_{1.2}Ni_{0.2-x}Co_{2x}Mn_{0.6-x}O_2$ powders: (a) $x = 0$, (b) $x = 0.01$, (c) $x = 0.02$, (d) $x = 0.03$, (e) $x = 0.04$, and (f) $x = 0.05$.

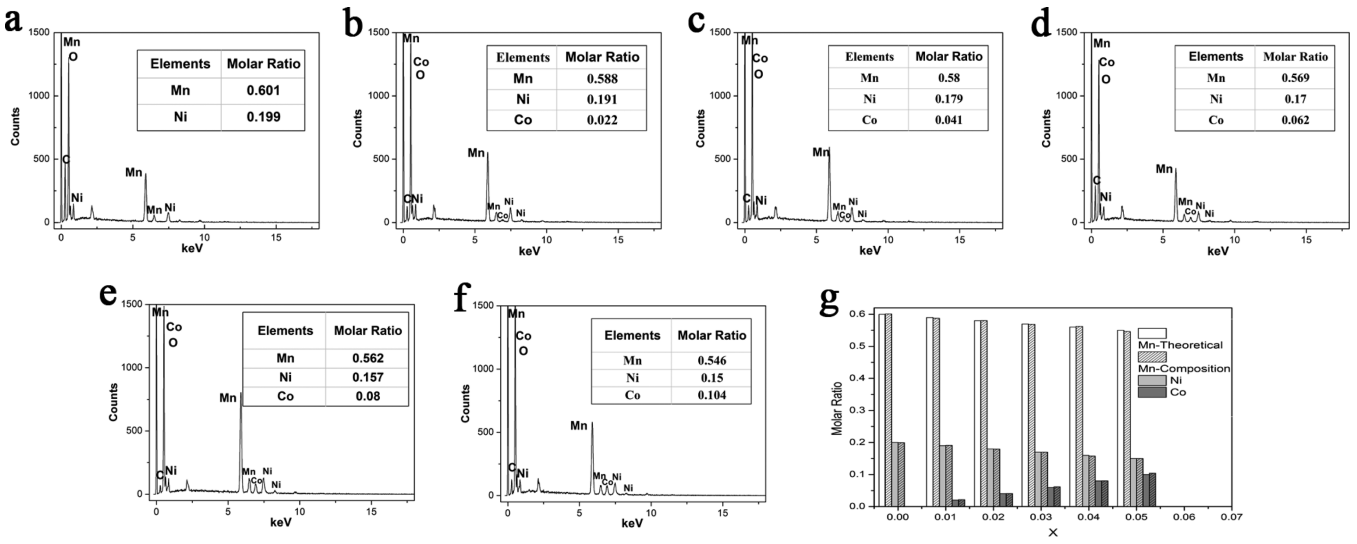

Figure 3. (a–f) EDX images of the $Li_{1.2}Ni_{0.2-x}Co_{2x}Mn_{0.6-x}O_2$ powders: (a) $x = 0$, (b) $x = 0.01$, (c) $x = 0.02$, (d) $x = 0.03$, (e) $x = 0.04$, and (f) $x = 0.05$ (inset tables in each panel show the molar ratios of the transition-metal elements). (g) Comparison of molar ratios measured by EDX and theoretical values.

the Co-0–Co-5 products, as presented in Figure 1a. All the samples show well-defined Bragg lines that correspond to the layered a-$NaFeO_2$ structure ($R\bar{3}m$ space group), except for some weak superlattices reflections at $2\theta \approx 20°–25°$ caused by Li^+/Mn^{4+} cation ordering in the transition-metal layers.[14] The cell parameters a and c (Figure 1c) decreased as the Co contents increased, which can be attributed largely to the fact that Co^{3+} (0.54 Å) has a similar ion radius to Mn^{4+} (0.53 Å), but is smaller than that of Ni^{2+} (0.69 Å) and Li^+ (0.76 Å).[34] This variation of cell parameters confirms the successful doping of Co into the Ni/Mn sites in the transition-metal layers.[35] In addition, clear peak splits of (006)/(102) (enlarged views in Figure 1b) and (018)/(110) reveal the highly ordered layered structure,[36] indicating that the small change in Co content has a negligible effect on the crystal structure and will not induce impurity phases.

3.2. Morphologies and EDX Spectra of the Samples. The morphologies of the as-synthesized Co-0–Co-5 powders were investigated by FESEM (see Figure 2). All the products demonstrate similar morphology with an average particle size between 100 nm and 200 nm. The works of Abraham et al. have shown that the low-temperature performance of electrode materials may be improved by decreasing the particle size or changing the particle morphology to reduce the high activation energy of the limiting process.[27] Neither changes of morphology nor particle size can be found in Figure 2 after Co doping; as such, any low-temperature performance differences in the final products can be directly related to the Co contents but not differences in particle size/morphology.

The composition and distribution of chemical elements in all the samples were determined by energy-dispersive X-ray (EDX) spectroscopy, as presented in Figures 3a–f. It can be seen that all the materials are composed of Co, Ni, and O species, while the elemental Co can only be detected in the doped samples. Figure 3g shows a comparison of the theoretical stoichiometry values and the calculated molar ratios of Mn, Ni, and Co for the synthesized materials. All the samples comply well with the target composition.

3.3. Electrochemistry Performances. To explore their low-temperature electrochemical properties of $Li_{1.2}Ni_{0.2-x}Co_{2x}Mn_{0.6-x}O_2$, the galvanostatic charge/discharge tests at 0.1 C were carried out at every 10 °C that ranges from

DOI: 10.1021/acsami.5b04514
ACS Appl. Mater. Interfaces 2015, 7, 17910–17918

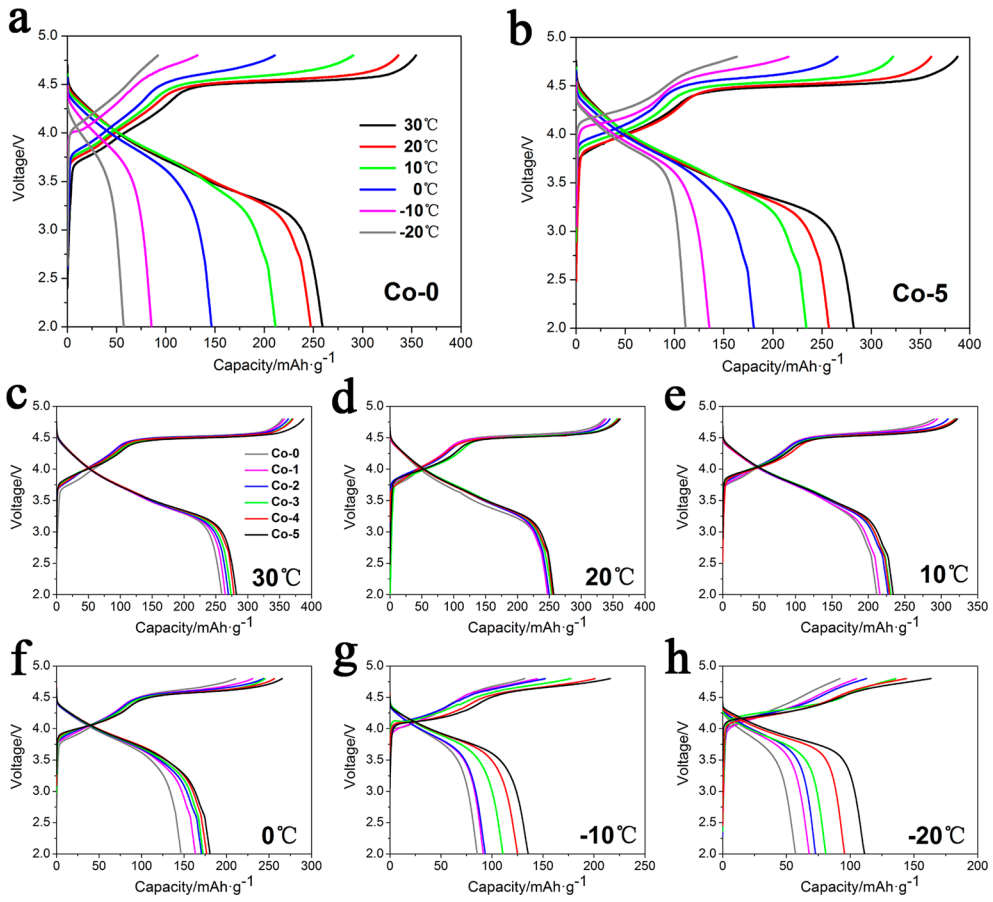

Figure 4. Initial charge−discharge curves at 0.1 C of the $Li_{1.2}Ni_{0.2-x}Co_{2x}Mn_{0.6-x}O_2$ powders under different temperatures (from 30 °C to −20 °C): (a) x = 0 and (b) x = 0.05. Initial charge−discharge curves at 0.1 C of the $Li_{1.2}Ni_{0.2-x}Co_{2x}Mn_{0.6-x}O_2$ powders with different Co contents at each temperature (x = 0−0.05): (c) 30 °C, (d) 20 °C, (e) 10 °C, (f) 0 °C, (g) −10 °C, and (h) −20 °C.

Table 1. Initial Discharge Capacity at 0.1 C under Different Temperatures (between 30 °C and −20 °C) of Samples Co-0−Co-5

	Initial Discharge Capacity (mAh g^{-1}) under Different Temperatures											
	30 °C		20 °C		10 °C		0 °C		−10 °C		−20 °C	
sample	total	<3.5 V	total	<3.5 V	total	<3.5 V	total	<3.5 V	total	<3.5 V	total	<3.5 V
Co-0	259.2	114.3	243.3	99.0	211.5	71.3	146.4	35.6	85.5	18.3	57.3	11.9
Co-1	264.7	118.9	245.0	99.7	215.9	74.7	163.3	44.9	91.5	19.0	67.9	12.1
Co-2	269.7	121.8	249.7	103.0	227.1	79.5	170.6	45.4	93.4	19.9	72.8	12.2
Co-3	273.8	122.8	253.7	105.5	230.8	80.9	172.3	46.0	110.8	23.9	80.9	13.9
Co-4	278.4	126.8	255.3	105.4	229.2	79.7	176.6	47.4	125.1	25.6	95.7	14.5
Co-5	282.2	130.3	256.9	106.3	234.0	83.7	180.6	50.8	135.5	27.7	111.3	16.8

30 °C to −20 °C. The initial charge−discharge curves of the sample Co-0 and Co-5 as representative examples for $Li_{1.2}Ni_{0.2-x}Co_{2x}Mn_{0.6-x}O_2$ powders are shown in Figures 4a and 4b. Both of them present the typical potential plateau of LLR materials at ∼4.5 V regions that originating from the electrochemical activation of Li_2MnO_3 phase, which leads to a low Coulombic efficiency that caused by partial elimination of the oxide-ion vacancies and lithium vacancies at the end of the first charge.[7−9,14−18,31−35,37] However, this plateau, at ∼4.5 V, is shortened as the temperature decreases, indicating an incomplete activation of Li_2MnO_3 phase, which should lead to a lower discharge capacity, accompanied by a reduction of $Mn^{3+/4+}$ inevitably. Meanwhile, there is also an increase of charge plateaus and a decline of discharge plateaus, accompanied by an expected decrease in the discharge capacity (see Table 1). Such an increase of electrode polarization and capacity drop may partly contribute to the increased interface reaction impedance, as well as slow ionic movement at low temperatures.[37,38] As we can see in Figures 4 a and 4b and in Table 1, the deterioration in the capacity and declination of discharge plateaus can be effectively mitigated after Co doping. Especially, the sloping region above ∼3.85 V during discharging is slightly affected by temperature changes after Co doping, as shown in Figure 4b.

Further comparison about initial charge/discharge curves at 0.1 C of $Li_{1.2}Ni_{0.2-x}Co_{2x}Mn_{0.6-x}O_2$ with different Co contents at each temperature is shown in Figures 4c−h. At 30 °C, the charge capacity increases from 354.2 mAh g^{-1} at x = 0 to 387.6 mAh g^{-1} at x = 0.05. The increase in charge capacity may arise from the enhanced oxygen loss caused by Co^{3+} substitution.[39] Accordingly, the reversible capacity from activation of Li_2MnO_3 component increases, as shown in Table 1 (capacity from

DOI: 10.1021/acsami.5b04514
ACS Appl. Mater. Interfaces 2015, 7, 17910−17918

sloping region below 3.5 V). Such an intrinsic enhancement in discharge capacity caused by Co doping is applicable to each temperature, but differences become much larger at lower temperatures. At 30 °C, the discharge capacity at 0.1 C is 259.2 mAh g^{-1} for Co-0, 264.7 mAh g^{-1} for Co-1, 269.7 mAh g^{-1} for Co-2, 273.8 mAh g^{-1} for Co-3, 278.4 mAh g^{-1} for Co-4, and 282.2 mAh g^{-1} for Co-5; however, at −20 °C, the discharge capacities are 57.3 mAh g^{-1}, 67.9 mAh g^{-1}, 72.8 mAh g^{-1}, 80.9 mAh g^{-1}, 95.7 mAh g^{-1}, and 111.3 mAh g^{-1}, respectively. The larger differences with lower temperature, in terms of discharge capacity, are shown in Figure 5a more directly. The

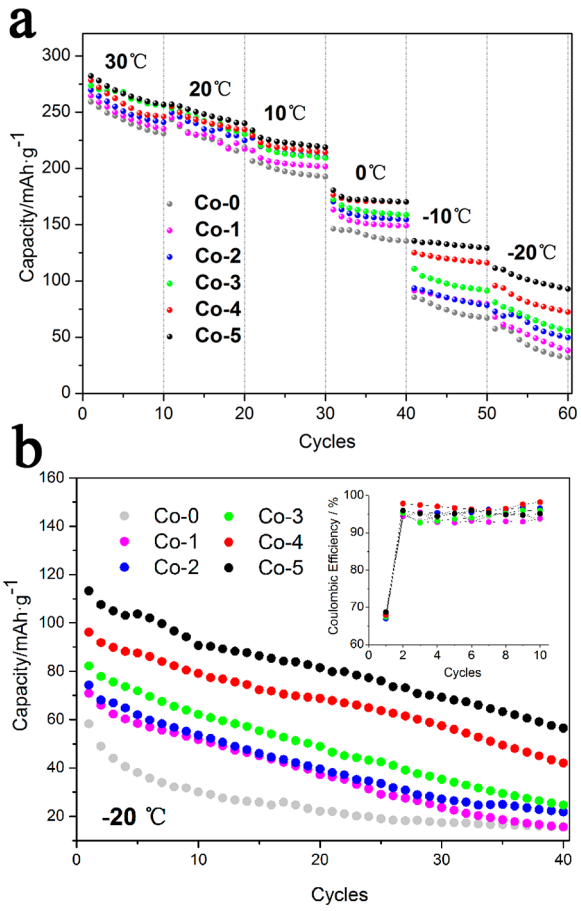

Figure 5. Cycle performance at 0.1 C of the $Li_{1.2}Ni_{0.2-x}Co_{2x}Mn_{0.6-x}O_2$ (x = 0, 0.01, 0.02, 0.03, 0.04, 0.05) powders at (a) each temperature for the first 10 cycles and (b) −20 °C; inset shows the Coulombic efficiency for the first 10 cycles.

electrochemical performance is greatly dependent on the temperature; there is an abrupt decrease in the capacity at every 10 °C drop. Nevertheless, every 10 cycles under each temperature, or even in a long-term cycling test at −20 °C (Figure 5b), doping more Co contents always leads to a superior capacity with higher capacity retention. Given that the capacity can be enhanced by Co doping intrinsically, as shown in Figure 4, capacity retention at different temperatures (Figure 6) is more convincing to reveal the role of Co doping in influencing the low-temperature performance of $Li_{1.2}Ni_{0.2-x}Co_{2x}Mn_{0.6-x}O_2$. As we can see in Figure 6a, difference in capacity retention become more evident below 0 °C. The initial discharge capacities at −20 °C of Co-0, Co-1, and Co-2 retain only 22.1%, 25.7%, and 27.0%, respectively, of that at 30 °C, while Co-3, Co-4, and Co-5 could maintain

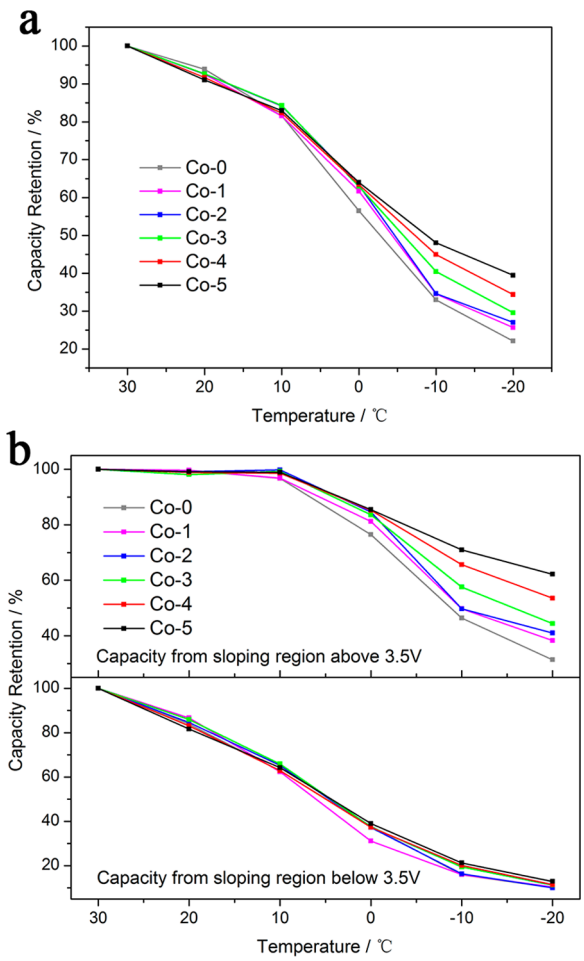

Figure 6. Discharge capacity retention of the $Li_{1.2}Ni_{0.2-x}Co_{2x}Mn_{0.6-x}O_2$ (x = 0, 0.01, 0.02, 0.03, 0.04, 0.05) powders at different temperatures: (a) total discharge capacity and (b) capacity from sloping region above/below 3.5 V.

29.5%, 34.4%, and 39.4%, respectively. As observed in Figures 4−6, the discharge capacities and operation voltages are drastically lowered, along with the decreased temperature, but their fading rate becomes slower with the increase of Co contents, especially below 0 °C, indicating a superior low-temperature performance that benefits from Co doping.

Discharge differential capacity (dQ/dV) plots are illustrated in Figure 7 to further investigate the influence from Co doping. It is clearly observed that the reduction peaks at ~3.85 V, which are generally considered as the reduction of Ni^{4+} or Co^{4+} ions in the rhombohedral phase,[40] is hardly affected by the testing temperature in the samples with high Co contents. In contrast, there's a drastic decrease in the peak height of Co-0−Co-2. The other cathodic peaks at ~3.35 V result from the reduction of Mn^{4+} in layered MnO_2 derived from Li_2MnO_3.[8,41] These peaks are more significantly dependent on operation temperature, instead of Co content. That means that the process about lithium reintercalation into a MnO_2-like component is more sensitive to temperature and shows limited effect after Co doping. Based on the previous reports,[8,14,30,41,42] we choose 3.5 V as a demarcation line to separate the discharge capacity into two parts for quantitative analysis: one is the capacity from sloping region above 3.5 V that contributes to the reduction of Ni^{4+} or Co^{4+}, and other is the remainder below 3.5 V due to reduction of Mn^{4+}. Their capacity retention under various

DOI: 10.1021/acsami.5b04514
ACS Appl. Mater. Interfaces 2015, 7, 17910−17918

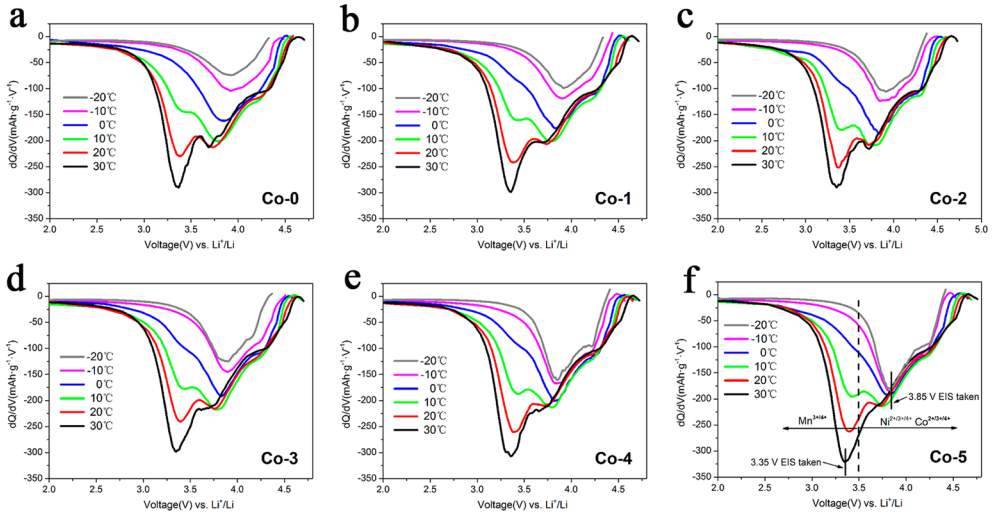

Figure 7. dQ/dV plots of the $Li_{1.2}Ni_{0.2-x}Co_{2x}Mn_{0.6-x}O_2$ (x = 0, 0.01, 0.02, 0.03, 0.04, 0.05) cells under various temperatures: (a) x = 0, (b) x = 0.01, (c) x = 0.02, (d) x = 0.03, (e) x = 0.04, and (f) x = 0.05.

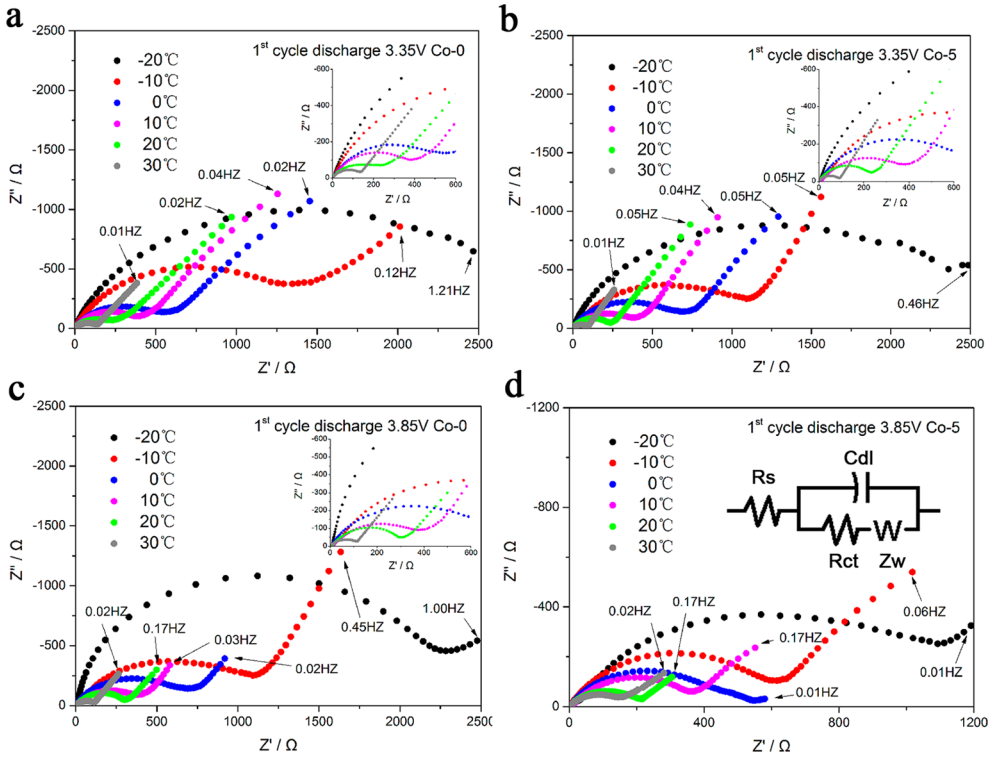

Figure 8. Nyquist plots of the Co-0 and Co-5 at different polarized states and temperatures: (a) Co-0 at 3.35 V, (b) Co-5 at 3.35 V, (c) Co-0 at 3.85 V, and (d) Co-5 at 3.85 V; inset in panel d shows a Voigt-type equivalent circuit.

temperatures is shown in Figure 6b. Clearly, the results of Figure 6b suggest that Co doping hardly affects the reduction process below 3.5 V, but plays a significant role in facilitating the reduction process above 3.5 V. In other words, the superior low-temperature performance caused by Co doping mainly results from the improved reduction process of Ni^{4+} or Co^{4+}. This conclusion is also supported by the results of X-ray photon spectroscopy (see Figure S1 in the Supporting Information).

3.4. Electrochemical Impedance Analysis. To further interpret this finding, impedance spectra of Co-0 and Co-5 were measured at different temperatures. Cells were discharged to 3.85 and 3.35 V in the initial cycle before the EIS test. The Nyquist plots for the electrodes that are given in Figure 8 show similar shapes. They are composed of a semicircle in the high frequency, which is associated with the charge transfer resistance (R_{ct}),[31,37] and a quasi-straight line in the low frequency. A possible equivalent circuit is proposed in Figure 8d. In this circuit, R_s corresponds to the solution resistance; R_{ct} and C_{dl} are the charge-transfer resistance and the double-layer capacitance at the electrode/electrolyte interface, respectively; and Z_w is the Warburg impedance associated with lithium diffusion in electrodes. Warburg impedance is in series with reaction resistance, since it is a Faradic component, while the double-layer capacitor operates in parallel to the faradic processes, since it is a non-Faradic component. Table 2

DOI: 10.1021/acsami.5b04514
ACS Appl. Mater. Interfaces 2015, 7, 17910−17918

Table 2. Value for the impedance parameter of Co-0 and Co-5 under Different Temperatures

	R_{ct} of Co-0 and Co-5 at Different Polarized States (Ω)			
	Co-0		Co-5	
temperature (°C)	3.85 V	3.35 V	3.85 V	3.35 V
30	160.1	100.7	157.9	90.3
20	269.2	156.9	194.8	144.6
10	388.7	263.4	275.0	235.8
0	699.1	511.7	421.3	468.9
−10	1260.1	960.2	628.3	801.3
−20	1880.0	2078.2	874.3	1820.9

summarizes the resulting impedance data calculated from the fitting equivalent circuit in Figure 8d. As shown in Table 2, R_{ct} shows a drastic increase with the decreased operation temperature, but the change rate is alleviated by Co doping, especially at 3.85 V. The R_{ct} value shows a negative correlation with the discharge capacity, which agrees well with the conclusion made by previous research that R_{ct} might be one of the main performance-limiting aspects at low temperature.[33] Therefore, it is rational that the more evident increase in R_{ct} of samples with lower Co contents when discharged to 3.85 V leads to a worse discharge capacity; whereas, when discharged to 3.35 V, the rate of increase of R_{ct} is hardly affected by the Co content, thus correlating little with the discharge capacity.

3.5. Activation Energy Analysis. The study on the activation energy (E_a) is also performed for a clear understanding of the kinetic trend of $Li_{1.2}Ni_{0.2-x}Co_{2x}Mn_{0.6-x}O_2$ after Co doping. The activation energy can be calculated by the temperature dependence charge transfer resistance (R_{ct}):[31,37]

$$\frac{\ln T}{R_{ct}} = \ln A - \frac{E_a}{RT}$$

Here, T is the absolute temperature, R_{ct} the charge transfer resistance, R the universal gas constant, and A the pre-exponential factor. According to this equation, E_a can be calculated from the slope of plots as shown in Figure 9, whose results reveal that the interface reaction of Ni^{4+} or Co^{4+} reduction at 3.85 V becomes easier after Co doping, whereas at 3.35 V, the activation energy E_a shows negligible change.

4. CONCLUSION

In this paper, $Li_{1.2}Ni_{0.2-x}Co_{2x}Mn_{0.6-x}O_2$ was successfully doped with different amounts of Co (x = 0−0.05) by a sol−gel method, followed by heat treatment. Their discharge capacities in a low-temperature environment were investigated. The discharge capacities and operation voltages are drastically reduced, along with the decreased temperature, but their fading rate becomes slower as the Co content increases. Activation energy analysis and EIS results reveal that such an enhancement benefits from the easier interface reaction of Ni^{4+} or Co^{4+} reduction after trace amounts of Co doping, which correlates little with the discharge process at ~3.35 V. The results of this paper prove the validity of reducing activation energy through ion doping in improvement of electrode materials' low-temperature performance, which could be expected to apply in other layered materials. In addition, further studies about improving low-temperature performance of lithium-rich cathode materials should focus on the process of lithium reintercalation into a MnO_2-like component.

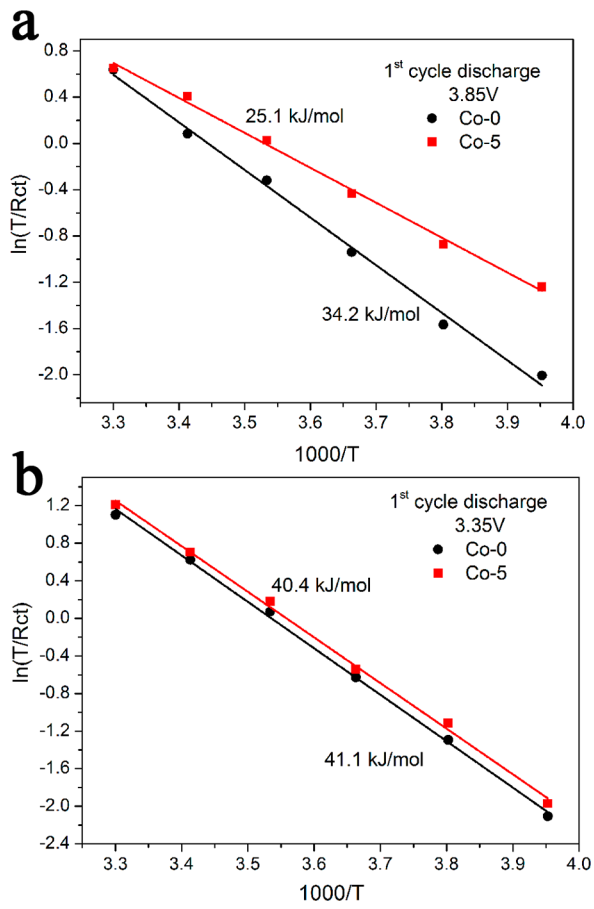

Figure 9. Activation energy of the first discharge processes of Co-0 and Co-5: (a) at 3.85 V and (b) at 3.35 V.

■ ASSOCIATED CONTENT

Supporting Information

The Supporting Information is available free of charge on the ACS Publications website at DOI: 10.1021/acsami.5b04514.

XPS spectra of Ni $2p_{3/2}$ for Co-0 and Co-5 electrodes (PDF)

■ AUTHOR INFORMATION

Corresponding Authors

*E-mail: suyuefeng@bit.edu.cn (Y. Su).
*E-mail: baoliying@bit.edu.cn (L. Bao).

Author Contributions

∇These authors contributed equally to this work.

Notes

The authors declare no competing financial interest.

■ ACKNOWLEDGMENTS

This work was funded by the Chinese National 973 Program (No. 2015CB251100), National Natural Science Foundation of China (Nos. 51472032 and 51202083), Program for New Century Excellent Talents in University (No. NCET-13−0044), the Special Fund of Beijing Co-construction Project (No. 20150939013), BIT Scientific and Technological Innovation Project (No. 2013CX01003).

DOI: 10.1021/acsami.5b04514
ACS Appl. Mater. Interfaces 2015, 7, 17910−17918

REFERENCES

(1) Whittingham, M. S. Lithium Batteries and Cathode Materials. *Chem. Rev.* **2004**, *104*, 4271−4302.
(2) Armand, M.; Tarascon, J.-M. Building Better Batteries. *Nature* **2008**, *451*, 652−657.
(3) Dunn, B.; Kamath, H.; Tarascon, J.-M. Electrical Energy Storage for the Grid: A Battery of Choices. *Science* **2011**, *334*, 928−935.
(4) Yang, Z.; Zhang, J.; Kintner-Meyer, M. C.; Lu, X.; Choi, D.; Lemmon, J. P.; Liu, J. Electrochemical Energy Storage for Green Grid. *Chem. Rev.* **2011**, *111*, 3577−3613.
(5) Goodenough, J. B.; Kim, Y. Challenges for Rechargeable Li Batteries. *Chem. Mater.* **2010**, *22*, 587−603.
(6) Goodenough, J. B. Rechargeable Batteries: Challenges Old and New. *J. Solid State Electrochem.* **2012**, *16*, 2019−2029.
(7) Li, N.; An, R.; Su, Y.; Wu, F.; Bao, L.; Chen, L.; Zheng, Y.; Shou, H.; Chen, S. The Role of Yttrium Content in Improving Electrochemical Performance of Layered Lithium-rich Cathode Materials for Li-ion Batteries. *J. Mater. Chem. A* **2013**, *1*, 9760−9767.
(8) Chen, L.; Su, Y.; Chen, S.; Li, N.; Bao, L.; Li, W.; Wang, Z.; Wang, M.; Wu, F. Hierarchical $Li_{1.2}Ni_{0.2}Mn_{0.6}O_2$ Nanoplates with Exposed {010} Planes as High-Performance Cathode Material for Lithium-Ion Batteries. *Adv. Mater.* **2014**, *26*, 6756−6760.
(9) Wu, F.; Li, N.; Su, Y.; Zhang, L.; Bao, L.; Wang, J.; Chen, L.; Zheng, Y.; Dai, L.; Peng, J.; Chen, S. Ultrathin Spinel Membrane-Encapsulated Layered Lithium-Rich Cathode Material for Advanced Li-Ion Batteries. *Nano Lett.* **2014**, *14*, 3550−3555.
(10) Mizushima, K.; Jones, P.; Wiseman, P.; Goodenough, J. B. Li_xCoO_2 ($0 < x < 1$). *Mater. Res. Bull.* **1980**, *15*, 783−789.
(11) Xu, B.; Qian, D.; Wang, Z.; Meng, Y. S. Recent Progress in Cathode Materials Research for Advanced Lithium Ion Batteries. *Mater. Sci. Eng., R* **2012**, *73*, 51−65.
(12) Lu, Z.; MacNeil, D.; Dahn, J. Layered Cathode Materials $Li[Ni_xLi_{(1/3-2x/3)}Mn_{(2/3-x/3)}]O_2$ for Lithium-Ion Batteries. *Electrochem. Solid-State Lett.* **2001**, *4*, A191−A194.
(13) Lu, Z.; Beaulieu, L.; Donaberger, R.; Thomas, C.; Dahn, J. Synthesis, Structure, and Electrochemical Behavior of $Li[Ni_xLi_{1/3-2x/3}Mn_{2/3-x/3}]O_2$. *J. Electrochem. Soc.* **2002**, *149*, A778−A791.
(14) Thackeray, M. M.; Kang, S.-H.; Johnson, C. S.; Vaughey, J. T.; Benedek, R.; Hackney, S. A. Hackney, S. Li_2MnO_3-Stabilized $LiMO_2$ (M = Mn, Ni, Co) Electrodes for Lithium-Ion Batteries. *J. Mater. Chem.* **2007**, *17*, 3112−3125.
(15) Yabuuchi, N.; Yoshii, K.; Myung, S.-T.; Nakai, I.; Komaba, S. Detailed Studies of a High-Capacity Electrode Material for Rechargeable Batteries, Li_2MnO_3−$LiCo_{1/3}Ni_{1/3}Mn_{1/3}O_2$. *J. Am. Chem. Soc.* **2011**, *133*, 4404−4419.
(16) Johnson, C. S.; Li, N.; Lefief, C.; Vaughey, J. T.; Thackeray, M. M. Synthesis, Characterization and Electrochemistry of Lithium Battery Electrodes: $xLi_2MnO_3\cdot(1-x)LiMn_{0.333}Ni_{0.333}Co_{0.333}O_2$ ($0 \le x \le 0.7$). *Chem. Mater.* **2008**, *20*, 6095−6106.
(17) Xu, B.; Fell, C. R.; Chi, M.; Meng, Y. S. Identifying Surface Structural Changes in Layered Li-Excess Nickel Manganese Oxides in High Voltage Lithium Ion Batteries: A Joint Experimental and Theoretical Study. *Energy Environ. Sci.* **2011**, *4*, 2223−2233.
(18) Gu, M.; Genc, A.; Belharouak, I.; Wang, D.; Amine, K.; Thevuthasan, S.; Baer, D. R.; Zhang, J.-G.; Browning, N. D.; Liu, J.; Wang, C. Nanoscale Phase Separation, Cation Ordering, and Surface Chemistry in Pristine $Li_{1.2}Ni_{0.2}Mn_{0.6}O_2$ for Li-Ion Batteries. *Chem. Mater.* **2013**, *25*, 2319−2326.
(19) Thackeray, M. M.; Johnson, C. S.; Vaughey, J. T.; Li, N.; Hackney, S. A. Advances in Manganese-Oxide 'Composite' Electrodes for Lithium-Ion Batteries. *J. Mater. Chem.* **2005**, *15*, 2257−2267.
(20) Wang, C.; Appleby, A. J.; Little, F. E. Low-Temperature Characterization of Lithium-Ion Carbon Anodes via Microperturbation Measurement. *J. Electrochem. Soc.* **2002**, *149*, A754−A760.
(21) Liao, X.-Z.; Ma, Z.-F.; Gong, Q.; He, Y.-S.; Pei, L.; Zeng, L.-J. Low-Temperature Performance of $LiFePO_4$/C Cathode in a Quaternary Carbonate-Based Electrolyte. *Electrochem. Commun.* **2008**, *10*, 691−694.
(22) Park, B.-C.; Kim, H.-B.; Bang, H. J.; Prakash, J.; Sun, Y.-K. Improvement of Electrochemical Performance of $Li[Ni_{0.8}Co_{0.15}Al_{0.05}]O_2$ Cathode Materials by AlF_3 Coating at Various Temperatures. *Ind. Eng. Chem. Res.* **2008**, *47*, 3876−3882.
(23) Tan, S.; Wang, L.; Bian, L.; Xu, J.; Ren, W.; Hu, P.; Chang, A. Highly Enhanced Low Temperature Discharge Capacity of $LiNi_{1/3}Co_{1/3}Mn_{1/3}O_2$ with Lithium Boron Oxide Glass Modification. *J. Power Sources* **2015**, *277*, 139−146.
(24) Nagasubramanian, G. Electrical Characteristics of 18650 Li-ion Cells at Low Temperatures. *J. Appl. Electrochem.* **2001**, *31*, 99−104.
(25) Plichta, E. J.; Behl, W. K. A Low-Temperature Electrolyte for Lithium and Lithium-Ion Batteries. *J. Power Sources* **2000**, *88*, 192−196.
(26) Choi, S. H.; Son, J.-W.; Yoon, Y. S.; Kim, J. Particle Size Effects on Temperature-Dependent Performance of $LiCoO_2$ in Lithium Batteries. *J. Power Sources* **2006**, *158*, 1419−1424.
(27) Abraham, D.; Heaton, J.; Kang, S.-H.; Dees, D.; Jansen, A. Investigating the Low-Temperature Impedance Increase of Lithium-Ion Cells. *J. Electrochem. Soc.* **2008**, *155*, A41−A47.
(28) Gaberscek, M.; Dominko, R.; Jamnik, J. Is Small Particle Size More Important than Carbon Coating? An Example Study on $LiFePO_4$ Cathodes. *Electrochem. Commun.* **2007**, *9*, 2778−2783.
(29) Huang, G.; Li, W.; Sun, H.; Wang, J.; Zhang, J.; Jiang, H.; Zhai, F. Polyvinylpyrrolidone (PVP) Assisted Synthesized Nano-$LiFePO_4$/C Composite with Enhanced Low Temperature Performance. *Electrochim. Acta* **2013**, *97*, 92−98.
(30) Shi, S.; Tu, J.; Tang, Y.; Zhang, Y.; Liu, X.; Wang, X.; Gu, C. Enhanced Electrochemical Performance of LiF-modified $LiNi_{1/3}Co_{1/3}Mn_{1/3}O_2$ Cathode Materials for Li-ion Batteries. *J. Power Sources* **2013**, *225*, 338−346.
(31) Yu, H.; Wang, Y.; Asakura, D.; Hosono, E.; Zhang, T.; Zhou, H. Electrochemical Kinetics of the $0.5Li_2MnO_3\cdot0.5LiMn_{0.42}Ni_{0.42}Co_{0.16}O_2$ 'Composite' Layered Cathode Material for Lithium-ion Batteries. *RSC Adv.* **2012**, *2*, 8797−8807.
(32) Qiu, B.; Wang, J.; Xia, Y.; Wei, Z.; Han, S.; Liu, Z. Temperature Dependence of the Initial Coulombic Efficiency in Li-rich Layered $Li[Li_{0.144}Ni_{0.136}Co_{0.136}Mn_{0.544}]O_2$ Oxide for Lithium-ions Batteries. *J. Power Sources* **2014**, *268*, 517−521.
(33) Yu, C.; Wang, H.; Guan, X.; Zheng, J.; Li, L. Conductivity and Electrochemical Performance of Cathode $xLi_2MnO_3\cdot(1-x)$-$LiMn_{1/3}Ni_{1/3}Co_{1/3}O_2$ ($x = 0.1, 0.2, 0.3, 0.4$) at Different Temperatures. *J. Alloys Compd.* **2013**, *546*, 239−245.
(34) Park, Y. J.; Hong, Y.-S.; Wu, X.; Kim, M. G.; Ryu, K. S.; Chang, S. H. Synthesis and Electrochemical Characteristics of $Li[Co_xLi_{(1/3-x/3)}Mn_{(2/3-2x/3)}]O_2$ Compounds. *J. Electrochem. Soc.* **2004**, *151*, A720−A727.
(35) Koga, H.; Croguennec, L.; Mannessiez, P.; Ménétrier, M.; Weill, F. o.; Bourgeois, L.; Duttine, M.; Suard, E.; Delmas, C. $Li_{1.20}Mn_{0.54}Co_{0.13}Ni_{0.13}O_2$ with Different Particle Sizes as Attractive Positive Electrode Materials for Lithium-ion Batteries: Insights into Their Structure. *J. Phys. Chem. C* **2012**, *116*, 13497−13506.
(36) Ohzuku, T.; Ueda, A.; Nagayama, M. Electrochemistry and Structural Chemistry of $LiNiO_2$ ($R\bar{3}m$) for 4 V Secondary Lithium Cells. *J. Electrochem. Soc.* **1993**, *140*, 1862−1870.
(37) Liu, X.; Li, H.; Yoo, E.; Ishida, M.; Zhou, H. Fabrication of $FePO_4$ Layer Coated $LiNi_{1/3}Co_{1/3}Mn_{1/3}O_2$: Towards High-Performance Cathode Materials for Lithium Ion Batteries. *Electrochim. Acta* **2012**, *83*, 253−258.
(38) Yoon, S.-J.; Myung, S.-T.; Sun, Y.-K. Low Temperature Electrochemical Properties of $Li[Ni_xCo_yMn_{1-xy}]O_2$ Cathode Materials for Lithium-Ion Batteries. *J. Electrochem. Soc.* **2014**, *161*, A1514−A1520.
(39) Xiang, X.; Knight, J. C.; Li, W.; Manthiram, A. Understanding the Effect of Co^{3+} Substitution on the Electrochemical Properties of Lithium-Rich Layered Oxide Cathodes for Lithium-Ion Batteries. *J. Phys. Chem. C* **2014**, *118*, 21826−21833.
(40) Arunkumar, T.; Wu, Y.; Manthiram, A. Factors Influencing the Irreversible Oxygen Loss and Reversible Capacity in Layered

DOI: 10.1021/acsami.5b04514
ACS Appl. Mater. Interfaces 2015, 7, 17910−17918

$Li[Li_{1/3}Mn_{2/3}]O_2$−$Li[M]O_2$ (M = $Mn_{0.5-y}Ni_{0.5-y}Co_{2y}$ and $Ni_{1-y}Co_y$) Solid Solutions. *Chem. Mater.* **2007**, *19*, 3067−3073.

(41) Wu, F.; Li, N.; Su, Y.; Shou, H.; Bao, L.; Yang, W.; Zhang, L.; An, R.; Chen, S. Spinel/Layered Heterostructured Cathode Material for High-Capacity and High-Rate Li-Ion Batteries. *Adv. Mater.* **2013**, *25*, 3722−3726.

(42) Chen, L.; Chen, S.; Hu, D.-Z.; Su, Y.-F.; Li, W.-K.; Wang, Z.; Bao, L.-Y.; Wu, F. Crystal Structure and Electrochemical Performance of Lithium-Rich Cathode Materials $xLi_2MnO_3\cdot(1-x)LiNi_{0.5}Mn_{0.5}O_2$ (x = 0.1−0.8). *Acta Phys. Chim. Sin.* **2014**, *30*, 467−475.

DOI: 10.1021/acsami.5b04514
ACS Appl. Mater. Interfaces 2015, 7, 17910−17918